Title

MICROSTRUCTURE, MECHANICAL PROPERTIES AND TWO-BODY ABRASIVE WEAR RESISTANCE OF AN Fe-3Cr-C BASED ULTRA-HIGH STRENGTH STEEL

Author

Yoon, Y.S.

Publication Date

1984-05-01

Lawrence Berkeley Laboratory
UNIVERSITY OF CALIFORNIA

Materials & Molecular Research Division

MICROSTRUCTURE, MECHANICAL PROPERTIES AND TWO-BODY ABRASIVE WEAR RESISTANCE OF AN Fe-3Cr-C BASED ULTRA-HIGH STRENGTH STEEL

Y.S. Yoon
(M.E. Thesis)

May 1984

Prepared for the U.S. Department of Energy under Contract DE-AC03-76SF00098

DISCLAIMER

LBL-17277

MICROSTRUCTURE, MECHANICAL PROPERTIES AND TWO-BODY ABRASIVE WEAR RESISTANCE OF AN Fe-3Cr-C BASED ULTRA-HIGH STRENGTH STEEL

Y.S. Yoon

Lawrence Berkeley Laboratory
University of California
Berkeley, California 94720

May 1984

This work was supported by the Director, Office of Energy Research, Office of Basic Energy Sciences, Materials Science Division of the United States Department of Energy, under Contract Number DE-AC03-76SF00098.

MICROSTRUCTURE, MECHANICAL PROPERTIES AND TWO-BODY ABRASIVE WEAR RESISTANCE OF AN FE-3CR-C BASED ULTRA-HIGH STRENGTH STEEL

Yoon Y.S.

M.E.

Dept. of Materials Science
and Mineral Engineering

Sponsor: U.S. Department of Energy

Gareth Thomas

Professor Gareth Thomas
Chairman of Committee

ABSTRACT

An ultra-high strength steel based on Fe-3Cr-0.4C for structural and abrasive applications has been designed and its structure-property relationships have been established. The micro-structure has been characterized as dislocated lath martensite containing fine carbides and surrounded by thin films of retained austenite. This results in excellent combination of mechanical properties and abrasion-resistance which are attractive in comparison to many commercial abrasion-resistant alloys. It has been shown also that the abrasion-resistance

mainly depends on the hardness.

Tempered martensite embrittlement occurs in the tempering temperature range of 300°C to 400°C and has been confirmed to be coincident with the decomposition of interlath retained austenite into stringers of coarse cementite. ε-carbide has been found in the as-quenched condition and in the 200°C tempered condition. The most likely sites for the formation of the cementite are shown to be the ε-carbide interfaces with the matrix and as the cementite particles grow, the ε-carbide particles gradually disappear.

MICROSTRUCTURE, MECHANICAL PROPERTIES AND TWO-BODY ABRASIVE WEAR RESISTANCE OF AN FE-3CR-C BASED ULTRA-HIGH STRENGTH STEEL

CONTENTS

I. INTRODUCTION

Ultra-high strength steels are mainly used in aircraft landing gear, rocket motor cases, missile bodies, bearings and shafts, armour plate, and other defense applications [1]. Since such steels have high hardness and consequently high abrasion resistance, they are also used in mining and mineral processing equipment such as buckets, chutes and loader shovels. Recently, the recognition of coal as an important source of energy has brought more significance to such steels.

Over the last decade, systematic investigations of alloying elements on the martensite structure and the mechanical properties have led to the development of an optimum composition of Fe/3Cr/2Mn/0.5 Mo/0.3C [2]. The microstructure of the alloy is characterized by dislocated lath martensite surrounded by interlath films of retained austenite [Fig. 1] and results in superior combinations of strength and toughness over many commercial alloys. However, it was designed to be neither an ultra-high strength steel nor a high abrasion-resistance steel. Hence, in this study ultra-high strength (UTS > 280 KSI) steel based on the above optimum composition has been designed and the structure-property relationship has been established.

The martensite tranformation in steels is perhaps the most exploited transformation to produce a variety of strength and toughness combinations at high strength levels. If controlled so that the inhomogeneous shear component occurs by slip rather than

by twinning, the martensite transformation is the most efficient method of producing a high density of dislocations, uniformily distributed in a fine-grained microstructure [3]. The dislocations are a necessary component for both strength and toughness. The main factor controlling this aspect of the transformation is composition, especially carbon content, which must be regulated to maintain Ms > 300°C [4] (Fig. 2). In this study two changes were made in the composition of Fe/3Cr/2Mn/.5Mo/.3C to increase the strength while not sacrificing the toughness much. Carbon content was raised to 0.4 wt. pct since the most common method of increasing the strength of martensite is through raising the carbon content. The Mn content was correspondingly reduced to 1 wt. pct to maintain Ms > 300°C to prevent the formation of twinned martensite coupled with the increase of carbon level.

11. EXPERIMENTAL PROCEDURE

A. MATERIALS PREPARATION

The alloy used in this investigation was supplied by Daido Steel Company, Japan. It was vacuum induction melted into 20 lb. ingots and subsequently rolled to 1 in. thick and 25 in. wide plates. The plates were homogenized under argon atmosphere at 1200°C for 24 hours before furnace cooling. Plane strain fracture toughness and Charpy V-notch impact toughness specimens were obtained from the plates. Round tensile specimens were also obtained (Fig. 3). The composition and the transformation temperatures determined by dilatometric measurements are listed in Table 1.

B. HEAT TREATMENTS

The heat treatment employed in this investigation is composed of austenitizing at 900°C for one hour, followed by quenching and tempering at various temperatures. The austenizing treatments were carried out in a vertical tube furnace under argon atmosphere. Oversized tensiles, Charpy and K_{IC} specimens were cut from their stocks and machined to blanks. After austenitizing treatment, specimens were quenched in agitated oil placed under the furnace. All the tempering treatments (200°C through 590°C) were carried out by immersing the specimens into a salt pot for one hour and then quenching into the agitated oil.

Final machining was done under flood cooling to avoid heating.

C. DILATOMETRY

A commercial dilatometer (Theta Dilatronic model) was used to obtain the cooling and heating curves. Phase transformation temperatures, viz., Ms, Mf (martensite start and finish) and As and Af (austenite start and finish) of the alloy were determined from these curves (Table 1).

D. MECHANICAL TESTING

(I) TENSILE AND HARDNESS TESTING

Round tensile specimens (Fig. 3a) with 1.25 in. gauge length were tested at room temperature in a 300 Kip capacity MTS testing machine at a cross-head speed of 0.04 in./min.

Hardness testing was performed on the Charpy specimens using the Rockwell hardness C scale.

(II) FRACTURE TOUGHNESS TESTING

Plane strain fracture toughness values were obtained by testing standard compact tension crack line loaded toughness specimens (Fig. 3c). After each heat treatment about 0.01 in. thickness was removed from each flat surface of the K_{IC} blanks.

The thickness of the specimens conformed to the ASTM specifications [5] for plane strain condition, viz.,

$$\text{thickness} > 2.5 \left(\frac{K_{IC}}{\sigma_y} \right)^2$$

The 300 Kip MTS machine was again used for fatigue precracking the specimens to a minimum crack length of about 0.05 in. Specimens then subsequently tested in the same machine to obtain the fracture toughness data. The orientation of crack propagation with respect to the long dimension of the bar stock is L-T [5].

(iii) CHARPY IMPACT TESTING

The size of the standard specimen is shown in Fig. 3b. Two or three specimens were tested for each heat treatment, and data points were taken as the average of these. Charpy impact testing was conducted on a 224 ft.-lbs. capacity impact device.

(iv) WEAR TESTING

Wear specimens, made from broken Charpy specimens, are hemisperically tipped cylindrical pins of 6.35 mm diameter and 20 mm length. The pins were hand cleaned in N-heptane to remove oil and dirt, and then ultransonically cleaned in ethyl alcholol for 10 minutes before testing.

Two-body, dry abrasive wear tests were conducted on a pin-on-disc wear machine which simulates high-stress abrasion. The wear pins were worn against abrasive paper for 10 revolutions at a rotational speed of 20 rpm under 1 kg deadweight load over a spiral track of 2.2 meters in length. The abrasive paper used was SiC of 120 grit. A break-in run was carried out prior to each of the three wear tests performed on each pin. The subsequent weight losses were measured on a Metler balance, capable of detecting weight losses of 0.01 mg and a mean value was calculated. The weight loss was then determined and converted to wear resistance as shown below:

Wear resistance = 1/ wear rate

$$= \frac{\text{length of wear path}}{\text{volume of material removed}}$$

$$= \frac{(\text{material density})\ (\text{length of wear path})}{\text{weight loss}} \text{ mm/mm}^3$$

E. METALLOGRAPHY

(i) OPTICAL METALLOGRAPHY

Specimens for optical metallography were cut mostly from

broken Charpy bars, mounted in cold-mount, abraded on silicon carbide papers down to 600 grit, and polished on 1 μm-diamond abrasive wheel. For revealing the martensitic microstructure specimens were etched in 5% nital solution and for revealing the prior austenite grain-boundaries they were etched in warm picric acid.

(II) SCANNING ELECTRON MICROSCOPY

Fractography was conducted on Charpy specimesn, using a ISI scanning electron microscope at 25 KV. The fracture surfaces were prepared by masking with a tape during cutting and specimen preparation. This tape was later dissolved in acetone.

(III) TRANSMISSION ELECTRON MICROSCOPY

Thin foils for TEM were obtained from Charpy specimens. About 20 mil thick slices were cut longitudinally from these specimens. After removing any oxide scale by cleaning, these slices were chemically thinned to about 5 mils in a solution of 4-5% HF in H_2O_2 at room temperature. Three mm-diameter discs were spark cut from these thinned slices. Finally, these thin foils were electropolished in a twin-jet electropolishing apparatus at room temperature using a chromic-acetic acid solution made of 75 gr CrO_3, 400 ml CH_3COOH and 21 ml distilled water. The polishing voltage varied between 40-45 volts, and that of current about 50-55 milliampers. Thin foils so obtained

were kept in ethyl-alchohol. Oxide layers cover the polished surfaces of the foils for very long time storage. Thse layers may be removed by repolishing the foil by holding it delicately with a pair of tweezers and carefully immersing it in agitated polishing solution for about a minute. Foils were then subsequently examined in Philips 301 microscope at an operating voltage of 100 KV.

III. RESULTS AND DISCUSSION

A. MICROSTRUCTURAL CHARACTERIZATION

(i) OPTICAL METALLOGRAPHY

Optical metallography was carried out to observe any variations in the gross features of microstructure, e.g., prior austentite grain size, coarse undissolved carbides or inclusions, if present, and so forth. Fig. 4 shows the optical microstructures after different etching conditions. For Fig. 4a to show the martensite structure nital solution was used and for Fig. 4b to show the prior austenite grain boundaries warm picric acid was used in etching. The structure consists of typical lath martensite although some indication of transition from lath to plate morphology is discernable (Fig. 4a). However, as will be shown in a later section, transmission electron microscopy revealed a predominately lath martensite structure. There were no undissolved carbides detected in the structure but some

inclusions were observed (Fig. 4b). Fig. 4b shows that the average size of the prior austenite grains is 35 μm.

(II) TRANSMISSION ELECTRON MICROSCOPY

Structural characterization by transmission electron microscopy was performed on the quenched and tempered conditions.

(a) AS-QUENCHED STRUCTURE

The morphology of martensite is basically dislocated lath type and the laths of average width about 0.3 μm are fairly straight and parallel to each other (Fig. 5).

There are two general morphologies of ferrous martensites, viz., dislocated lath and twinned plates. Since the twinned martensite has lower toughness than the dislocated martensite [6], to obtain high toughness, one of the requirements in designing martensitic alloys is to avoid inducing twinning. Several explanations for the transition from lath to plate martensite have been proposed. Thomas [7] summarized some of the factors thought to be important in controlling the martensite morphologies and they are 1) composition, especially carbon, 2) Ms temperatures, 3) strength of the martensite, and 4) austenite stacking fault energy. Considering all of the above factors depend on composition, generally one would say that the higher is the solute content the greater is the probability of forming twinned plates. Carbon seems to be the most potent of the

alloying elements in promoting twinning. Carbon is also the most potent strengthener of steel. Thus, the stronger the steel the more difficult it is for slip to occur and then twinning is preferred. In this alloy design program, therefore, the carbon content is carefully increased with adjusting the Mn content so as not to promote twinning significantly.

Three important structural variations, viz., microstructural twinning, auto-tempered carbides and retained austenite were observed. Although the substructure of the martensite remains essentially dislocated, a small amount (about 15 pct of the laths observed) of the well-known $\{112\}_\alpha$ microtwins [8] (Figs. 5,8) were observed. Since the martensite substructure closely resembles that in shock-loaded materials [9] and in fcc metals as the shock pressure is increased, twins are formed when the dislocation density has attained some critical value [10,11], the microtwins observed in martensite laths may have been induced because the critical dislocation density may have been exceeded. A more likely reason for twinning is due to accomodation deformation subsequent to the transformation.

The observed auto-tempered carbides are identified as ε-carbides (Figs. 6,7). It is not clear under what conditions ε-carbides forms or what morphology it has. However, ε-carbide is described as 'cross-hatched' [12,13] carbide because of its appearance in thin foil electron micrographs. In the as-quenched or the low-temperature tempered martensites many workers found evidence to suggest a transition carbide phase. Jack [14] first established the structure of the phase as h.c.p. and named it ε-

carbide. He proposed the following orientation relationship between martensite and the carbide.

$$(001)_{\alpha} \; //(0001)_{\varepsilon}$$

$$(101)_{\alpha} \; //(1011)_{\varepsilon}$$

and further suggested that the growth direction of carbide particles would be $\langle 110 \rangle_{\alpha}$. The orientation relationship suggested by Jack has been experimentally confirmed by a single-crystal x-ray technique [15] and thin foil electron microscopy [8,12,16,17]. However, the $\langle 110 \rangle_{\alpha}$ growth direction proposed by Jack has not been confirmed. Several investigations [12,16,17] report that ε-carbide grows either in $\langle 100 \rangle_{\alpha}$ directions while Murphy and Whiteman [8] observed ε-carbide needles growing in $[211]_{\alpha}$ with $(211)_{\alpha} \; //(100)_{\varepsilon}$, a relationship which they suggest leads to minimization of interfacial and strain energy. The observation in this study (Fig. 6,7) agrees with Jack's relationship and the $[211]_{\alpha}$ growing direction suggested by Murphy and Whiteman.

The presence of retained austenite between the martensite laths was observed (Fig. 8). Though the mechanisms for retention of the high temperature fcc austenite phase are not fully understood, generally, one would expect that fcc stabilizing elements should promote the retention of austenite. Thomas and Rao [8] have shown that in alloys whose bulk Ms and Mf temperatures are above room temperature, austenite can be retained at room temperature only in the presence of interstitial C, which is the strongest fcc stabilizer. Interstitial C can stabilize austenite in several ways [19] and some of them are 1)

chemical stabilization, ii) thermal stabilization, and ii) mechanical stabilization. In these mechanisms, the redistribution of solute element, especially carbon, is significant as was indicated by lattice imaging methods [26]. Sarikaya et al. [27] have showed the carbon partition between austenite and martensite with higher carbon levels at the interface by field ion-atom probe analysis, which indicates the importance of carbon on the interface mobility during the growth of the laths suggested by Schoen et al. [28]. The careful modification of composition in this study seems not to change the morphology and the amount of retained austenite of the reference steel significantly.

(b) TEMPERED STRUCTURES

Tempering at 200°C does not change the as-quenched structure significantly except for the precipitation of cementite (indicated by arrows in Fig. 9). The cementite platelets are about 200 A wide and 0.2 μm long. The arrays of cementite are paralled to <111> while those of ε-carbide are paralled to $<211>_{\alpha}$ (Fg. 9). Fig. 9 also shows that the most likely sites for the formation of the cementite are the ε-carbide interfaces with the matrix and as the cementite particles grow, the ε-carbide particles gradually disappear.

The retained austenite is still stable at this temperature. Fig. 10 shows the extensive amount of retained austenite in the 200°C tempered structure. The stabilization of retained

austenite at this tempering temperature may be due to the redistribution of carbon atoms (chemical stabilization) and interface dislocations pinned by interstitials or small carbides (thermal stabilization). Since martensite is oversaturated in carbon and retained austenite is not, carbon atoms migrate from martensite to retained austenite, which stabilizes retained austenite chemically [27]. At the same time, many carbon atoms accumulate at the semicoherent interface between martensite and retained austenite during migration and form Cottrell atmospheres to pin interface dislocations. These pinned interface dislocations would directly inhibit interface motion and thus inhibit stress relaxation in martensite or retained austenite.

The microstructures of the specimen tempered at 300°C were quite different from the microstructures of the as-quenched and 200°C tempered specimens. Extensive cementite precipitation or coarsening both inside the lath and at the lath boundaries were observed (Fig. 11). The interlath cementite stringers at the lath boundaries are the products of the decompostion of retained austenite (tempered martensite embrittlement). This decomposition arises because of thermally activated nucleation and growth whereby cementites nucleate directly on the interface, where carbon achieves a high concentration value [27]. The easy growth direction of the cementites is along the film of retained austenite rather than into the martensite. As the carbon atoms diffuse into the newly formed cementites along the interface, there must be carbon depleted regions in austenite.

These regions then transform into ferrite probably by a shear mechanism [29].

(iii) CORRELATION OF MECHANICAL PROPERTIES, ABRASION RESISTANCE, AND MICROSTRUCTURES

The mechanical properties and the abrasion resistance of the alloy designed in this study are summarized in Tables 2,3 and the values are plotted as a function of tempering temperature in Figs. 12, 13. The alloy loses hardness and strength rapidly between the as-quenched and 200°C tempered condition, whereas the 0.3C reference steel does not lose these properties significantly. This means that the hardness changes during tempering are very dependent on carbon content.

Significant improvements in the impact toughness and the plane strain fracture toughness upon 200°C tempering may be due to the precipitation of very fine carbides within almost all of the laths and also attributed to more mechanically stable austenite films at the lath boundaries. The mechanisms of increased crack propagation resistance in the presence of retained austenite include [9]: i) crack branching, resulting in a more tortuous crack propagation and the consequent increase in energy expended, ii) crack blunting, as a result of plastic flow in austenite resulting in a decrease in stress concentration, and iii) transformation induced plasticity in which case the transformation of retained austenite to martensite under stress/strain in the plastic zone ahead of a crack relieves

stress concentrations. In all the cases, the effectiveness of retained austenite in improving toughness increases with its stability to transformation under mechanical stress/strain.

The abrasion resistance has been known to be directly proportional to the bulk hardness of annealed pure metals [21-24], because hardness controls the penetration depth of the abrasives. The overall trends of the change of abrasion resistance with varying tempering temperature (Fig. 13) is very similar to those of hardness (Fig. 12) in this study as well. However, the decreasing rate of abrasion resistance upon 200°C tempering is lower than that of hardness. This may be explained in terms of toughness. The significant improvement of the toughness upon 200°C tempering seems to alleviate the decreasing rate of abrasion resistance, while the hardness decreases rapidly.

Upon 300°C tempering the hardness, and the toughness decrease drastically, the decrease of hardness is due to the loss of tetragonality of martensite [25] since tetragonality of martensite wholly depends on the carbon content and in this temperature range the extensive formation of cementite reduces the carbon content of the matrix. The decrease of toughness is due to the tempered martensite embrittlement. This embrittlement is not the classic intergranular embrittlement due to impurity segregation or precipitation at the the grain boundaries. The embrittlement is transgranular (Fig. 14b) and is attributed to the decomposition of retained austenite with the formation of interlath cementite (or M_3C) films (Fig. 11) [30-32]. These

interlath carbides may either provide crack nucleation sites and/or restriction of fracture to particlar laths [30,32]. At 200°C tempering, the predominant fracture mode is dimpled rupture (Fig. 14a) while at 300°C tempering it is quasicleavage (Fig. 14b).

The decreasing slope of abrasion resistance is steeper than that of hardness upon 300°C tempering. This may be due to the overlapping effect of the tempered martensite embrittlement on the decrease of hardness.

IV. CONCLUSIONS

As a part of continuing alloy design program, ultra-high strength steel based on Fe/3Cr/C composition has been optimized for structural and abrasion-resistant applications. Excellent combinations of mechanical properties and abrasion-resistance were obtained (Fig. 15,16). The main conclusions of this investigation are as follows:

1) Increasing the carbon content from 0.3 wt. pct to 0.4 wt. pct with decreasing Mn content from 2 wt. pct to 1 wt. pct on the reference composition, Fe/3Cr/2Mn/0.5Mo/0.3C, does not change the microstructural features significantly, and as a result the combination of mechanical properties and the abrasion resistance are much superior to the equivalent commercial steels (Fig. 15,16). The excellent abrasion resistance may result from the combination of strength (hardness) and toughness.

2) Careful increase of the carbon content from 0.3 wt. pct to 0.4 wt. pct with adjustment of the Mn content augments the abrasion-resistance by about 20% more than that of the 0.3 C reference steel at the 200°C tempered condition (Fig. 13).

3) Comparing the tempering response of the abrasion-resistance with the mechanical properties (Figs. 12,13) shows that the abrasion-resistance correlates well with the hardness compared to Charpy toughness. Therefore, Charpy toughness is not

a primary factor in 2-body abrasion-resistance.

4) Tempered martensite embrittlement (TME) occurs in the tempering temperature range 300 to 400°C and is coincident with the decomposition of interlath retained austenite into stringers of coarse cementite at these boundaries. However, temper embrittlement does not occur in all the tempering temperature range.

5) Auto-tempered ε-carbide has been found in the as-quenched condition. The analysis of diffraction pattern supports the Jack's orientation relationship listed below:

$$(011)_{\alpha} \; //(0001)_{\varepsilon}$$

$$(101)_{\alpha} \; //(1011)_{\varepsilon}$$

and agrees with Murphy and Whiteman in the growth direction of ε-carbide of $[2\bar{1}1]_{\alpha}$ direction.

6) The most likely sites for the formation of the cementite are the ε-carbide interfaces with the matrix and as the cementite particles grow, the ε-carbide particles gradually disappear.

Acknowledgements

The author would like to express his sincere appreciation to Professor Gareth Thomas for his support and guidance throughout the course of this investigation. Deep appreciation is extended to Dr. R.M. Fisher for his encouragement, enthusiasm and manifold discussions. Respect and appreciation is expressed to Professor I. Finnie for the discussions and review of the manuscript.

S. Kwok's helpful suggestions, cooperation with the wear testing will long be appreciated. Sincere feelings of appreciation are expressed to Jean for her writing consultation and typing the manuscript.

The author remains forever obligated to his wife for her help, cooperation, understanding and endearment.

This work was supported by the Director, Office of Energy Research, Office of Basic Energy Sciences, Materials Science Division of the United States Department of Energy, under contract number DE-AC03-76SF00098.

REFERENCES

1. Pickering: Physical Metallurgy and Design of Steels. Applied Science Publishers LTD, London, 1978. 127.

2. Sarikaya, M., Steinberg, G. B. and Thomas, G., Met. Trans., 1982, 13A, p. 2227.

3. Thomas, G.: Fundamental Aspects of Structural Alloy Design, R. I. Jafee and B. A. Wilcox, eds., Plenum Publishing, 1977, p. 331.

4. Thomas, G.: Iron and Steel Intl., 1973, 46, p. 451.

5. Standard Method of Test for "Plain Strain Fracture Toughness of Metallic Materials," designation E 399-7, Annual ASTM Standards, 1973, p. 960.

6. Das, S. K. and Thomas, G.: Trans. ASM., 1969, 62, p. 659.

7. Thomas, G.: Met. Trans., 1971, 2, p. 2373.

8. Murphy, S. and Whiteman, J. A.: Met. Trans., 1979, 1, p. 843.

9. Leslie, W.C., Stevens, D. W., and Cohen, M.: High Strength Materials, p. 382, J. Wiley, New York, N. Y., 1965.

10. Nolder, R.L. and Thomas, G.: Acta Met., 1964, 12, p. 227.

11. Johari, O. and Thomas, G.: Acta Met., 1954, 12, p. 1153.

12. Tekin, E. and Kelly, P. M.: Precipitation from Iron Base Alloys, A.I.M.E., 1965, p. 173.

13. Wells, M.G.H.: Acta Met., 1964, 12, p. 389.

14. Jack, K.H.: J. Iron St. Inst., 1951, 26, p. 169.

15. Arbusoz, M.P. and Khayenko, B.V.: Fiz. Metal Metalloved., 1962, 13, p. 294.

16. Hale, K.F. and McLean, D.: J. Iron St. Inst., 1963, 201, p. 337.

17. Chilton, J. and Kelly, P.M.: Acta Met., 1968, 16, p. 637.

18. Thomas, G. and Rao, B.V.N.: Martensite Transformation, p. 57, Academy of Science, Kiev, USSR, 1978.

19. Rao, B.V.N. and Thomas, G.: Met. Trans., 1980, 11A, p. 441.

20. Speich, G. R. and Leslie, W.C.: Met. Trans., 1972, 3, p. 1043.

21. Khruschov: Inst. of Mech. Eng., Proc. Conf. on Lubrication and Wear, London, England, 1957, p. 665.

22. Misra, A.: Ph. D. Thesis, University of California, Berkeley, California, September 1979.

23. Richardson, R.C.: Wear, 1968, 11, p. 245.

24. Kwok, S.: M.S. Thesis, University of California, Berkeley California, January 1982.

25. Bain, E.D.: J. Iron Steel Inst., 1955, 181, p. 193.

26. Roa, B.V.N. and Thomas, G.: Proc. Intl. Conf. on Martensitic Transformation, ICOMAT-79, Cambridge, Mass., MIT Press, 1979, p. 12.

27. Sarikaya M., Thomas, G., Barnard, S.J. and Smith, G.D.W.: Proc. Intl. Conf. on Solid Phase Transformations, Aaronson, H.I., Laughlin, D.E., Sekera, R.F. and Wayman, C.M., eds., TMS-AIME, Warrendale, PA, 1982, p. 1421.

28. Schoen, F.J. and Owens, W.S.: Met. Trans., 1971, 2 p. 2431.

29. Thomas, G. and Sarikaya, M.: Proc. Int. Conf. on Solid Phase Transformations, Aaronson, H.I., Laughlin, R.F., Sekerka, R.F. and Wayman, C.M. eds., TMS-AIME, Warrendale, PA, 1982, p. 999.

30. Thomas, G.: Met. Trans., 1978, 9A, p. 439.

31. McMahon, J.A. and Thomas, G.: Proc. Int. Conf. on the Microstructure and Design of Alloys, Inst. of Metal, London, 1973, 1, p. 180.

32. Sarikaya, M., Jhingan, A. K. and Thomas, G.: Met. Trans., 1983, 14A, p. 1121.

Table 1. Alloy Composition and Transformation Temperature

Composition, Wt Pct									Temperature °C			
Cr	C	Mn	Mo	Si	Cu	P	S	Fe	Ms	M_f	As	A_f
3.02	0.39	1.01	0.51	0.01	0.01	0.003	0.006	Bal.	310	200	780	820

Table 2. Mechanical Properties

Tempering Temperature (°C)	Hardness (RC)	0.2 Pct Offset YS		UTS		Pct Elongation		Kic		Charpy V-notch Energy	
		ksi	MPa	ksi	Mpa	Total	(Uniform)	ksi-in	MPa-$m^{\frac{1}{2}}$	ft-lb	N-m
AQ	58.5	270	1860	350	2412	6.4	(3.0)	58.0	64.4	9.6	13.0
200	54.5	250	1723	300	2067	6.9	(3.3)	80.0	88.8	19.7	26.7
300	50.2	220	1516	255	1757	6.2	(2.9)	-	-	13.2	17.9
400	49.5	218	1502	250	1723	5.7	(2.7)	-	-	12.3	16.7
500	46.5	200	1378	225	1550	9.8	(3.1)	-	-	17.4	23.6
590	36.3	145	999	162	1116	15.0	(4.1)	-	-	65.4	88.7

Table 3. Wear Properties

Tempering Temp.(°C)	Weight Loss per One pass (mg)	Wear Resistance (mm/mm^3)
AQ	1.56	11100
200	1.64	10560
300	1.95	8880
400	2.03	8530
500	2.10	8250
590	2.2	7870

FIGURE CAPTIONS

Fig. 1. Scheme showing the desired duplex microstructure consisting of lath marensite and thin films of retained autenite at ultra-high strength level.

Fig. 2. Scheme showing relationship between substructure of martensite (inhomogeneous shear), and transformation temperature at ultra-high strength level.

Fig. 3. Sketches of (a) round tensile specimen, (b) Charpy impact toughness specimen, (c) K_{IC} fracture toughness specimen.

Fig. 4. Optical micrographs of the as-quenched structure. (a) shows the martensite structure and (b) shows the prior austenite grain boundaries.

Fig. 5. A bright field (BF) micrograph showing characteristic configuration of laths and packets in the as-quenched structure.

Fig. 6. (a) BF, (b) DF, (c) SAD pattern and (d) the

and 7. corresponding indexed pattern of as-quenched structure revealing the auto-tempered ε-carbide.

Fig. 8. (a) BF, (b) DF, (c) SAD pattern and (d) the corresponding indexed pattern of as-quenched structure. Extensive amount of retained austenite in the form of films can be seen in (b).

Fig. 9. (a) and (b) DF of the 200°C tempered structure revealing the ε-carbide and the cementite together. Notice that the growing directions of the ε-carbide

and the cementite are different and that the most likely sites for the formation of the cementite are ε-carbide interfaces with the matrix.

Fig.10. DF of the 200° tempered structure revealing the extensive amount of retained austenite in the form of films.

Fig.11. (a) BF and (b) DF of the 300°C tempered structure, (b) is showing the decomposition of retained austenite into the interlath cementite stringers and the coarse intralath cementite.

Fig. 12. Hardness and Charpy impact energy vs. tempering temperature curves.

Fig. 13. Wear resistance vs. tempering temperature curve.

Fig. 14. Fractographs of (a) 200°C tempered condition and (b) 300°C tempered condition.

Fig. 15. Comparison of toughness to strength relations in the experimental alloy and equivalent commercial alloys. (a) Charpy impact energy vs. tensile strength and (b) plane strain fracture toughness vs. tensile strength.

Fig. 16. Comparison of wear resistance in the experimental alloy and commercial abrasive of equivalent structural alloys.

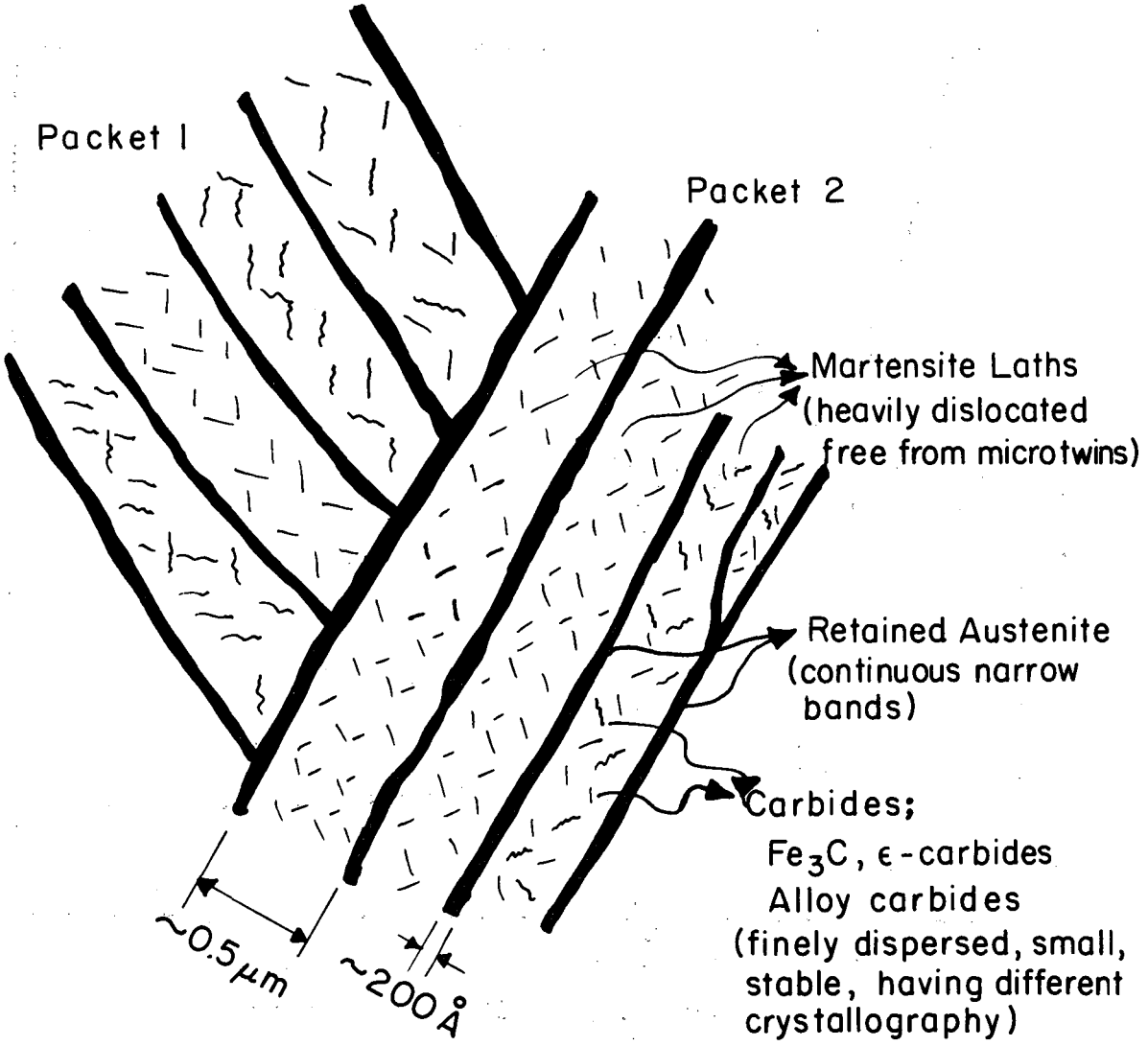
Packet I
Packet 2
Martensite Laths
(heavily dislocated
free from microtwins)
Retained Austenite
(continuous narrow
bands)
Carbides;
Fe_3C, ε-carbides
Alloy carbides
(finely dispersed, small,
stable, having different
crystallography)
~0.5μm
~200Å
XBL794-6146

Fig. 1

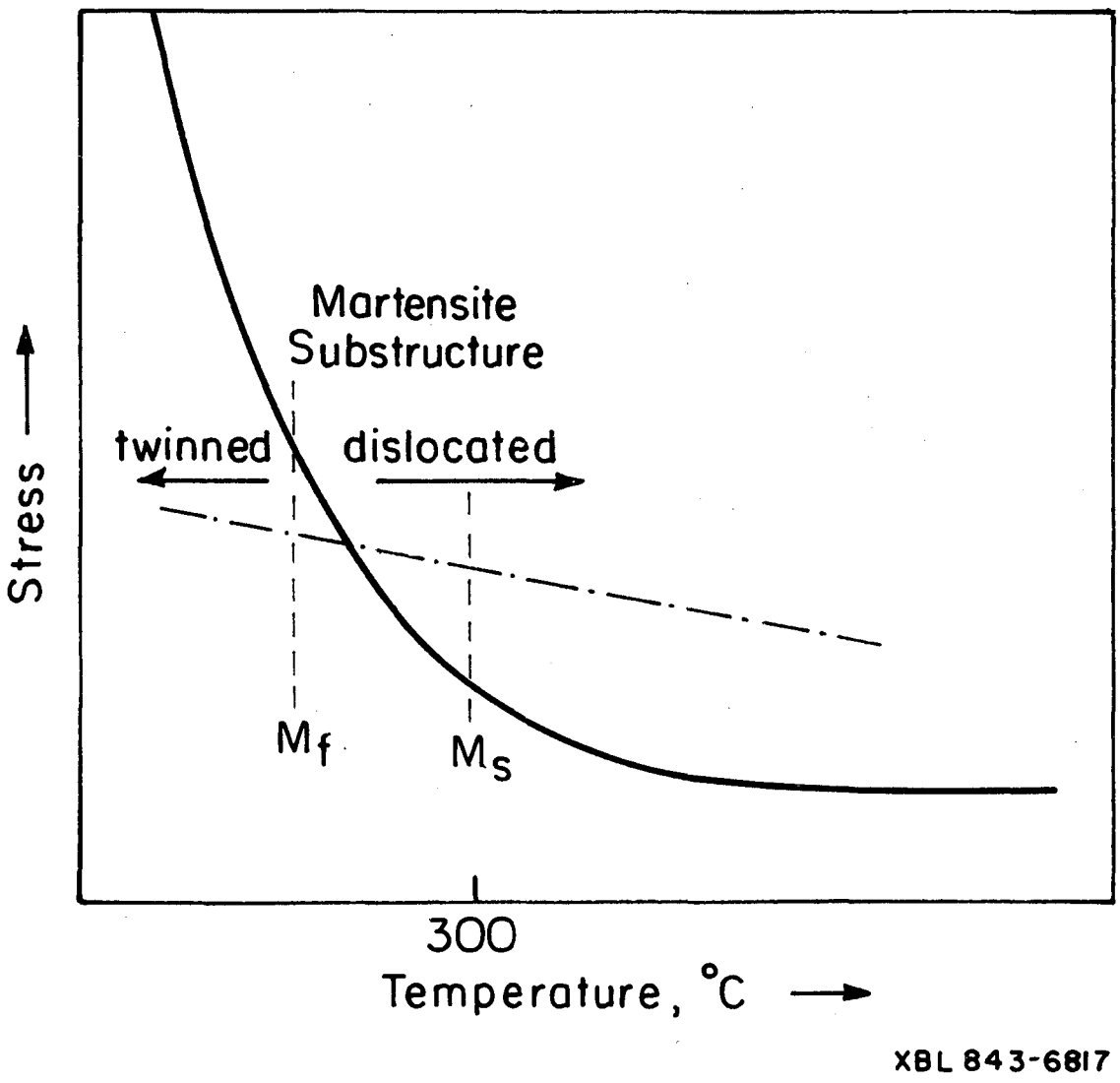
Martensite
Substructure
twinned
dislocated
Stress
M_f
M_s
300
Temperature, °C
XBL 843-6817

Fig. 2

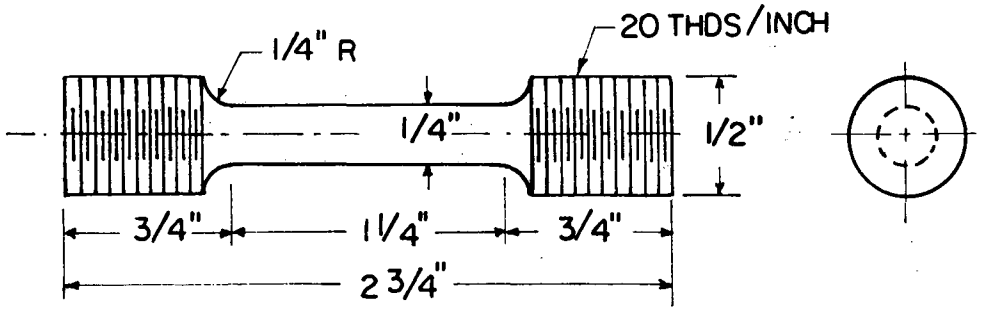

A. ROUND TENSILE SPECIMEN

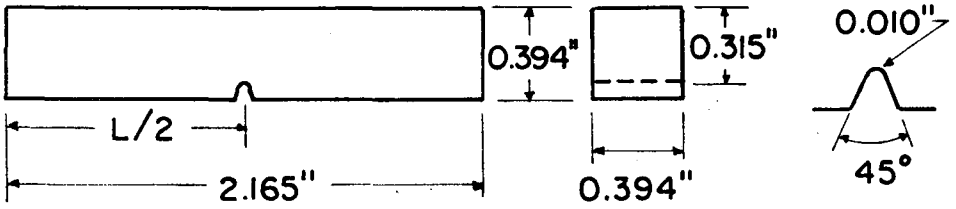

B. CHARPY V-NOTCH IMPACT SPECIMEN

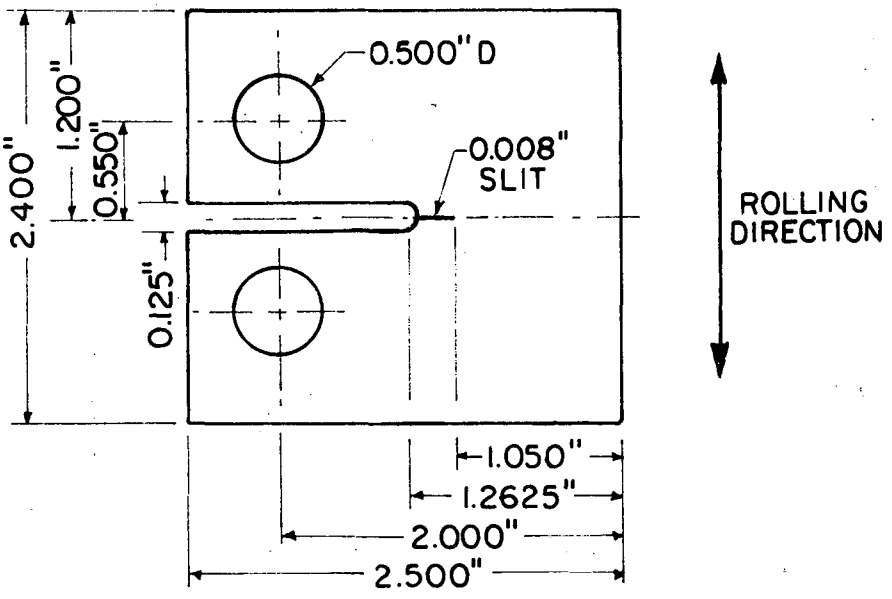

C. FRACTURE TOUGHNESS SPECIMEN

XBL843-6827

Fig. 3

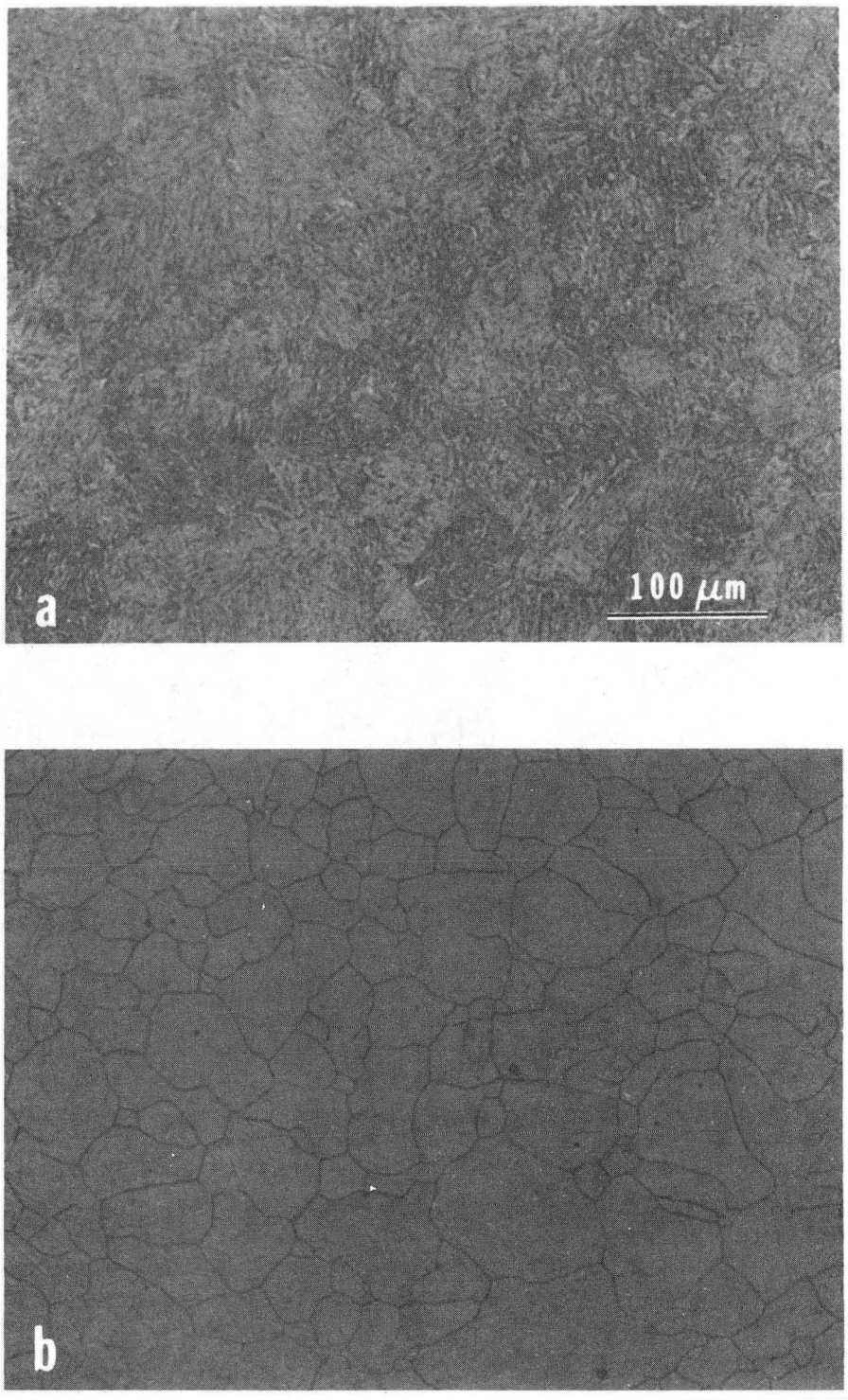

XBB 837-6000

Fig.4

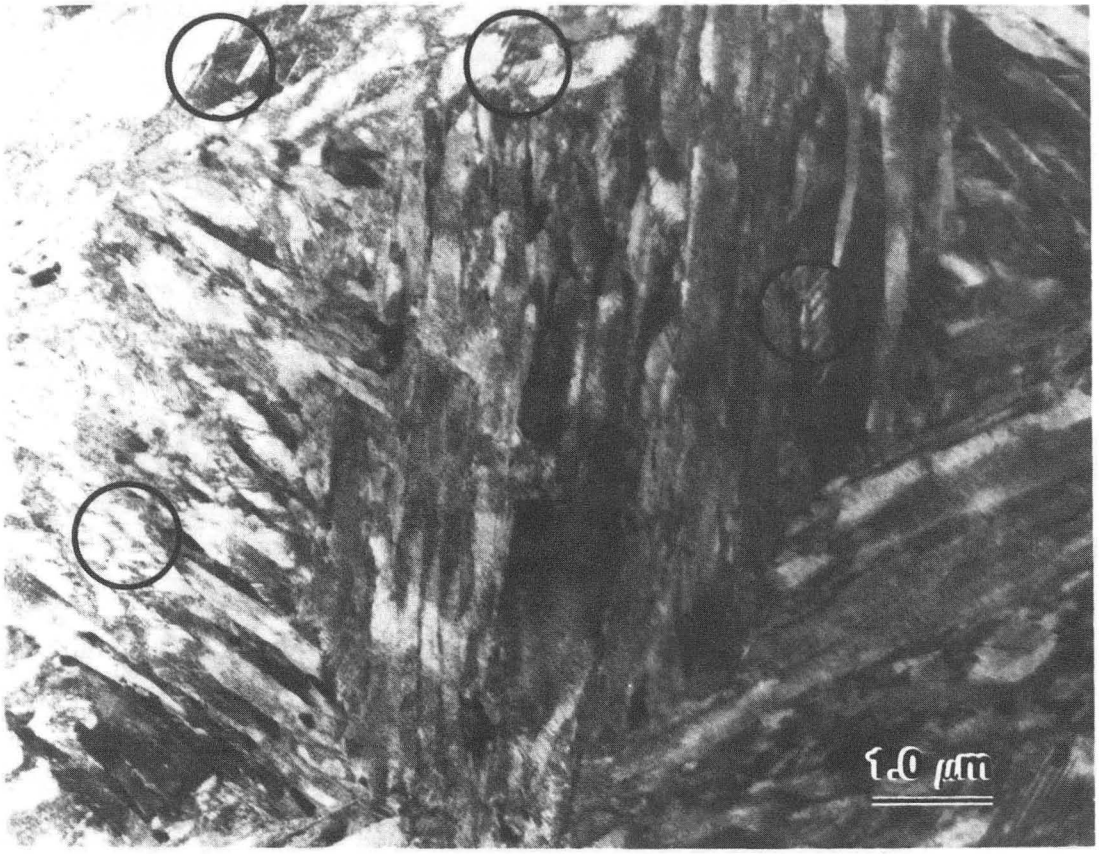

XBB 837-5998

Fig. 5

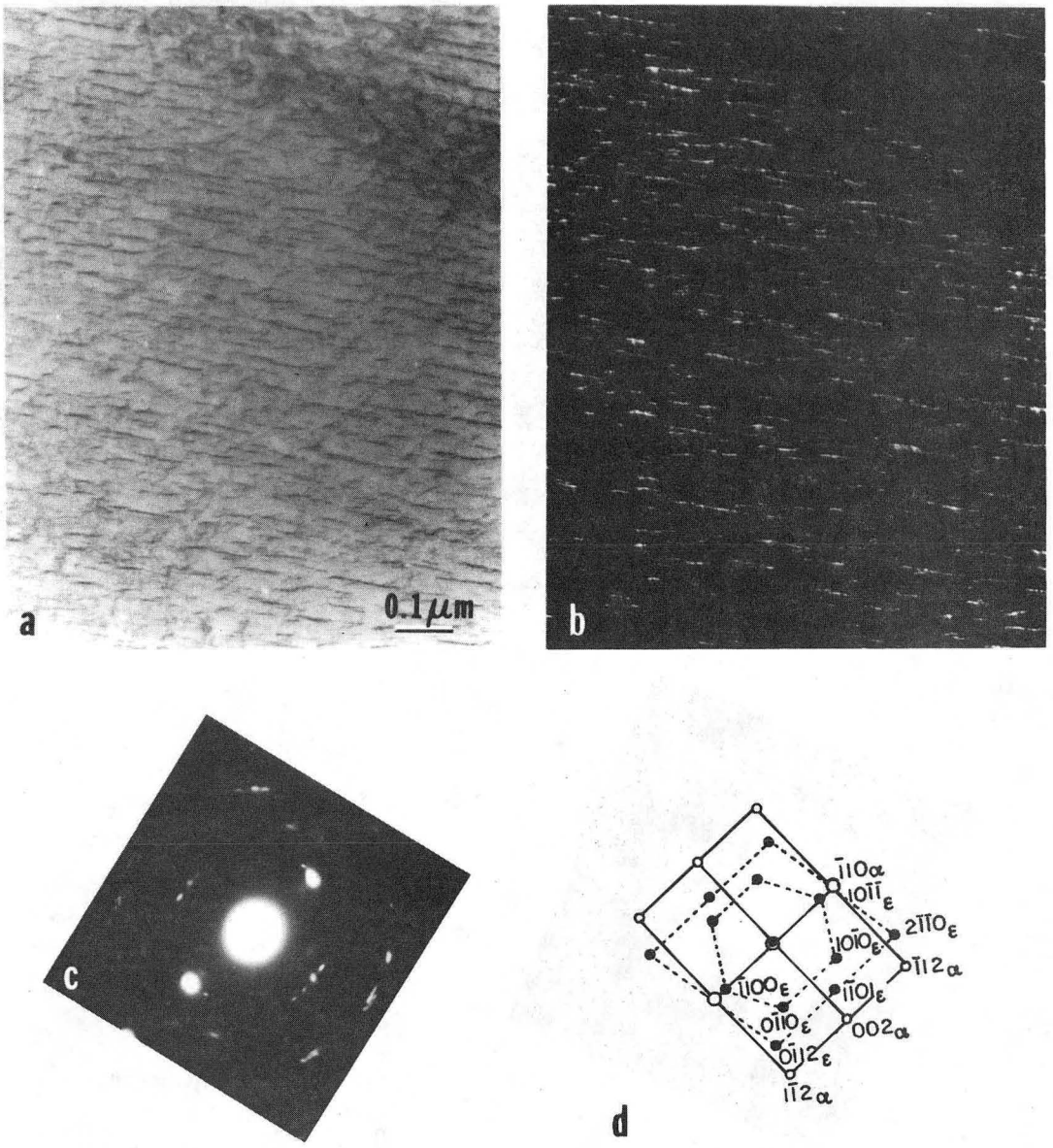

XBB 837-6173

Fig. 6

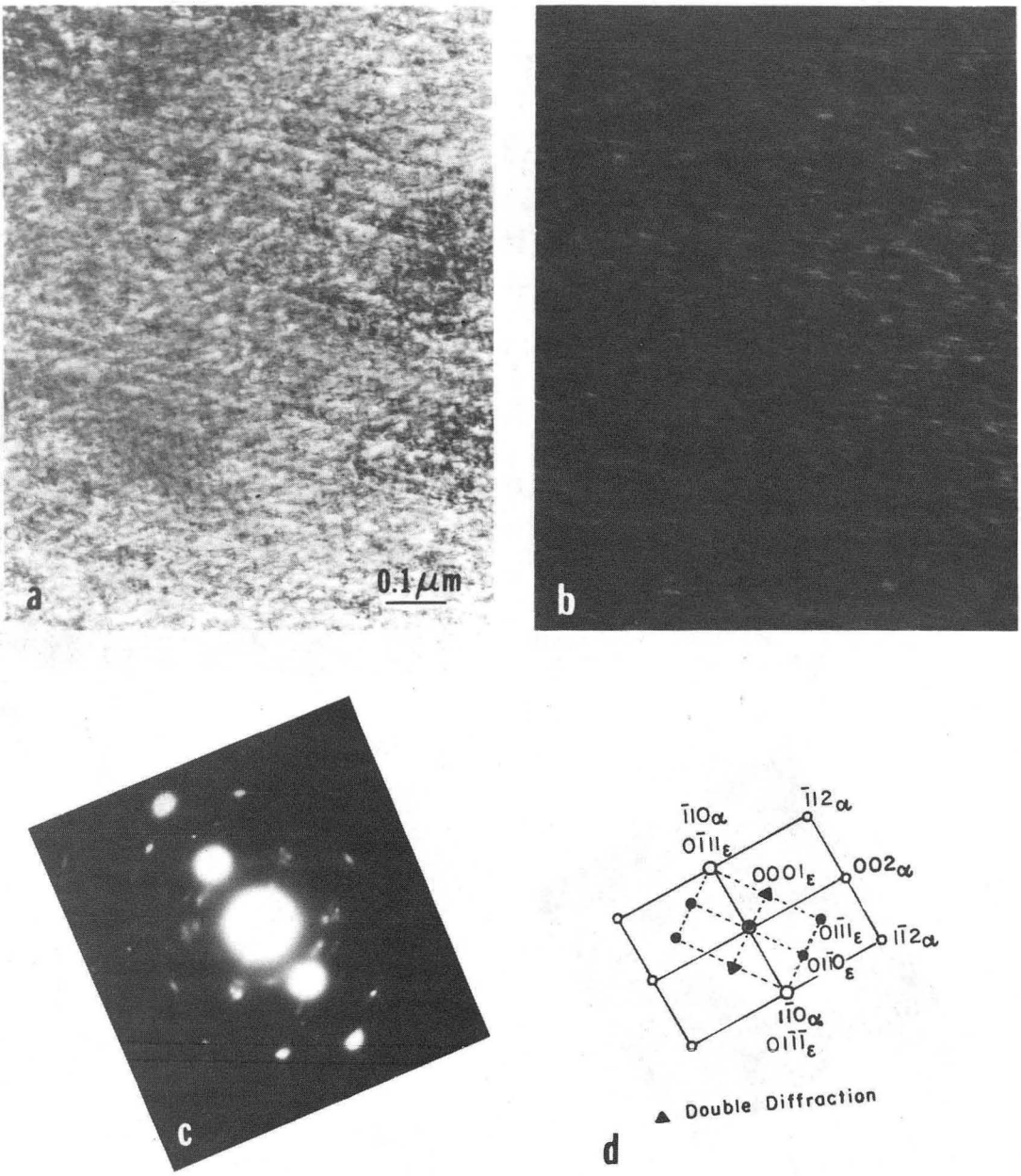

XBB 837-6174

Fig. 7

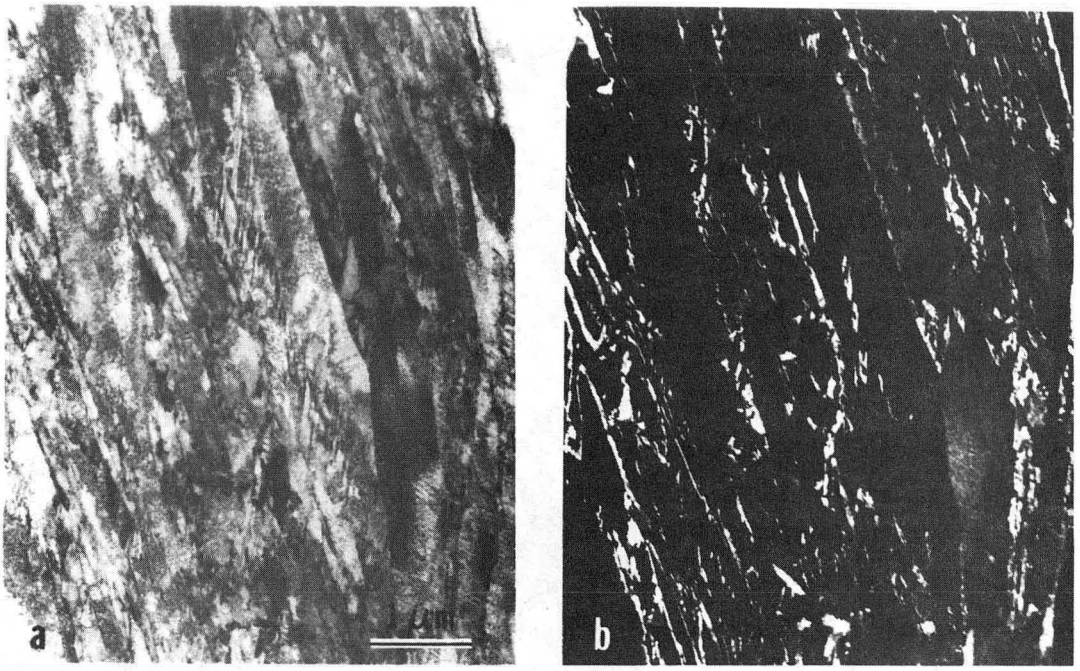

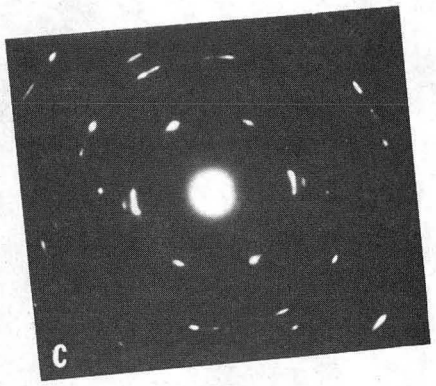

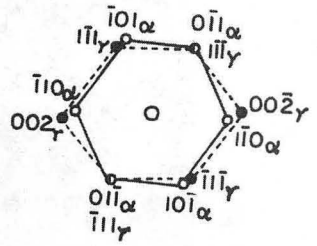

d

XBB 837-6172

Fig. 8

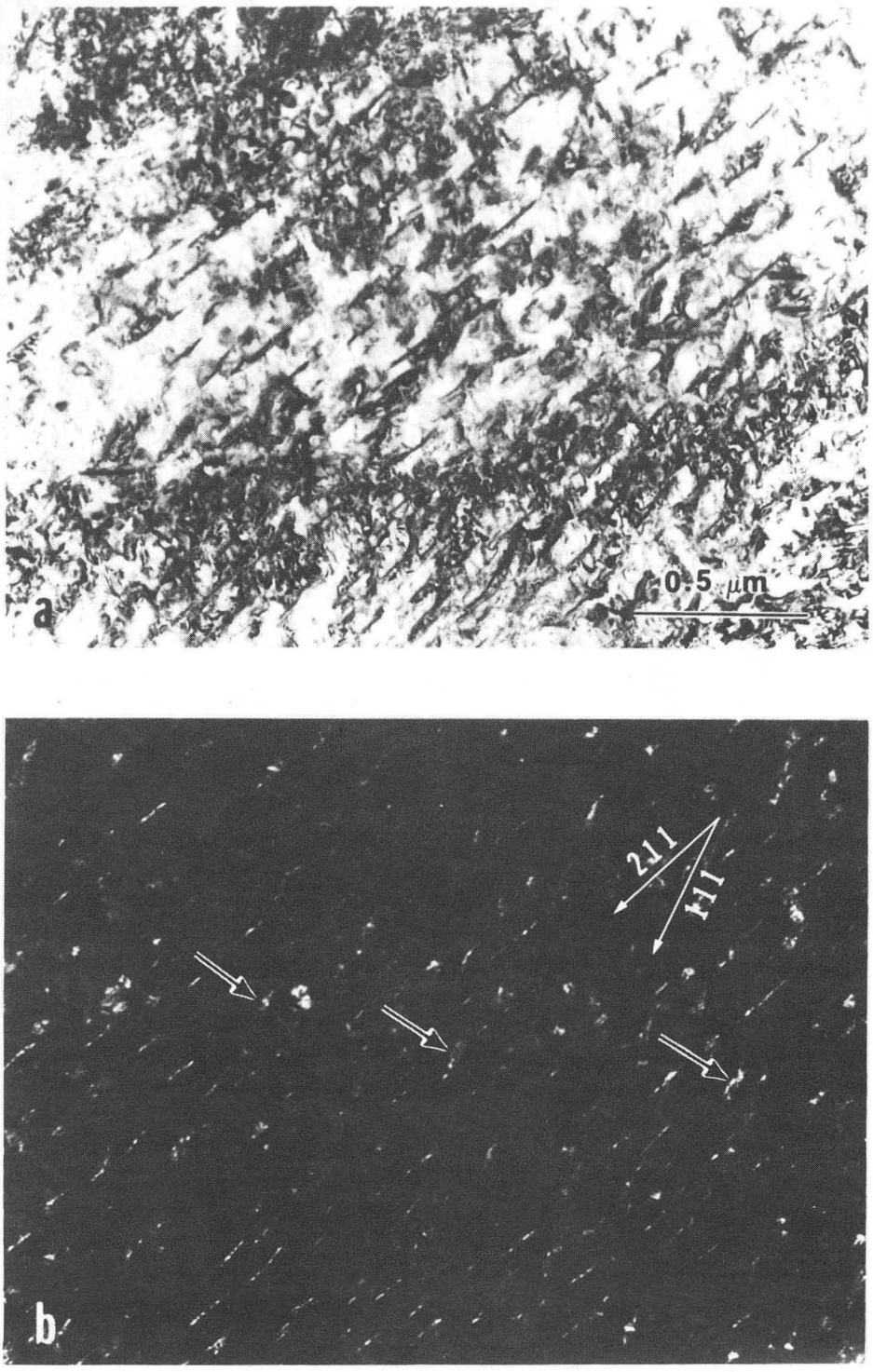

XBB 837-5997

Fig. 9

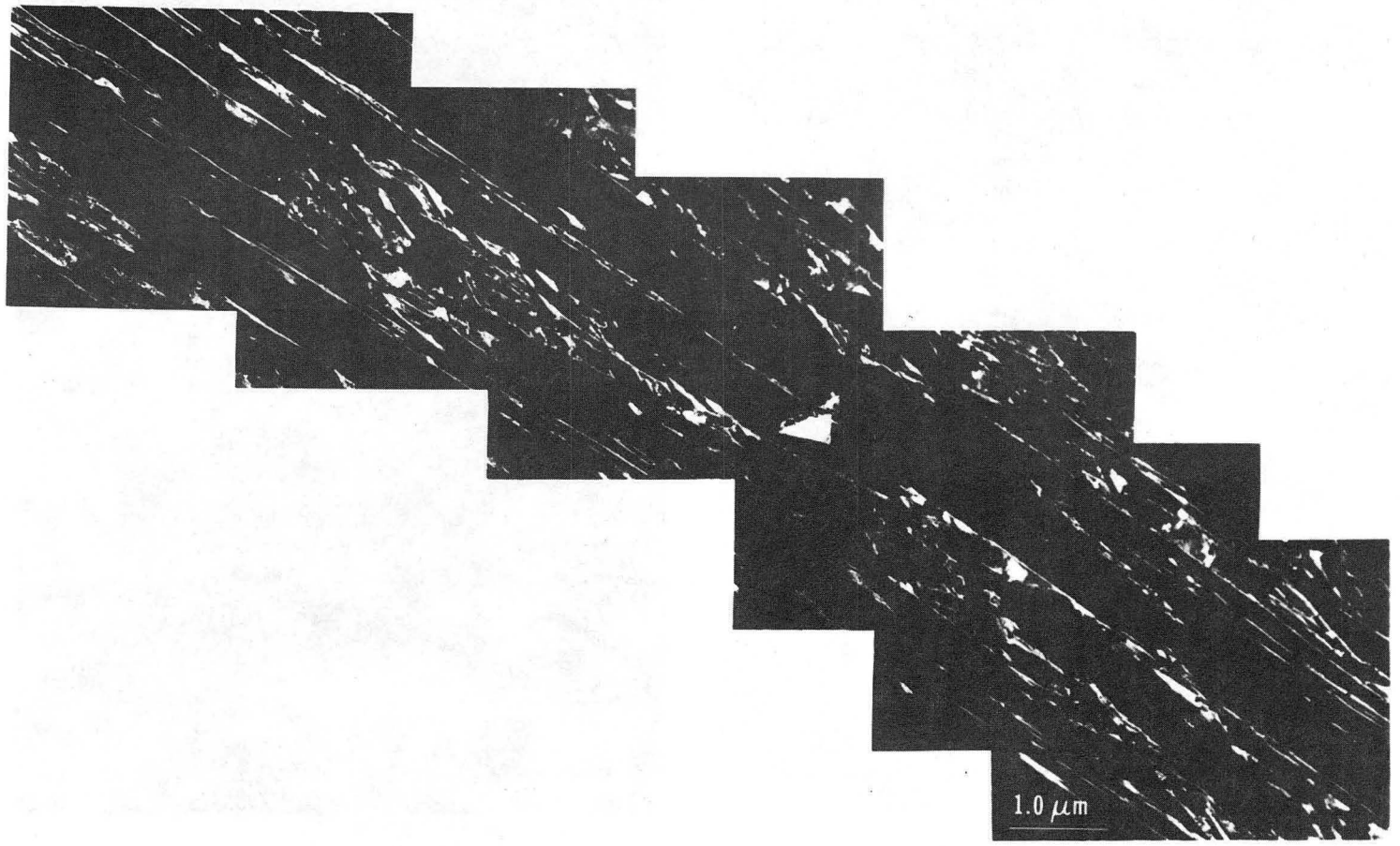

XBB 837-6001

Fig. 10

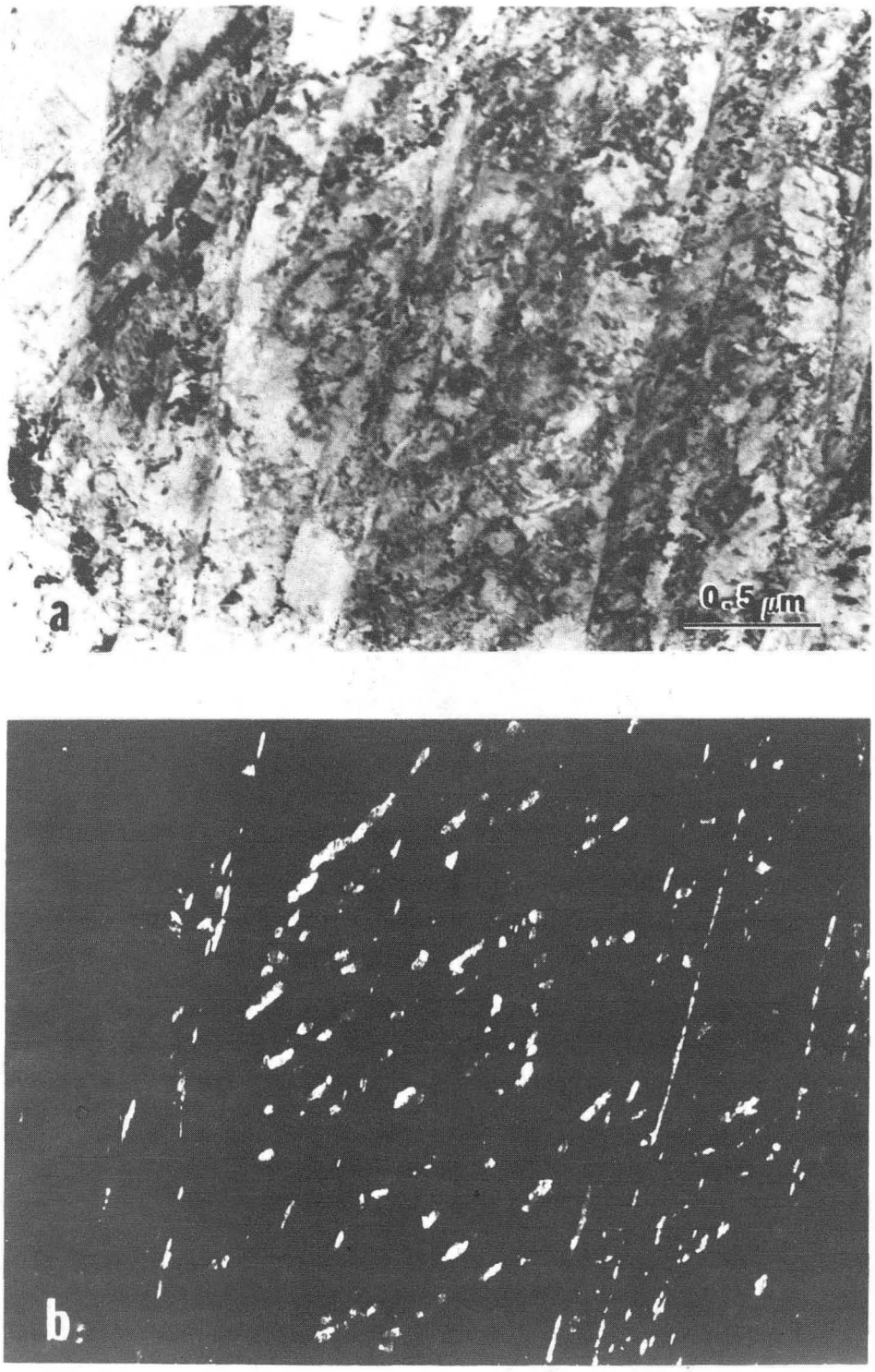

XBB 837-5999

Fig. 11

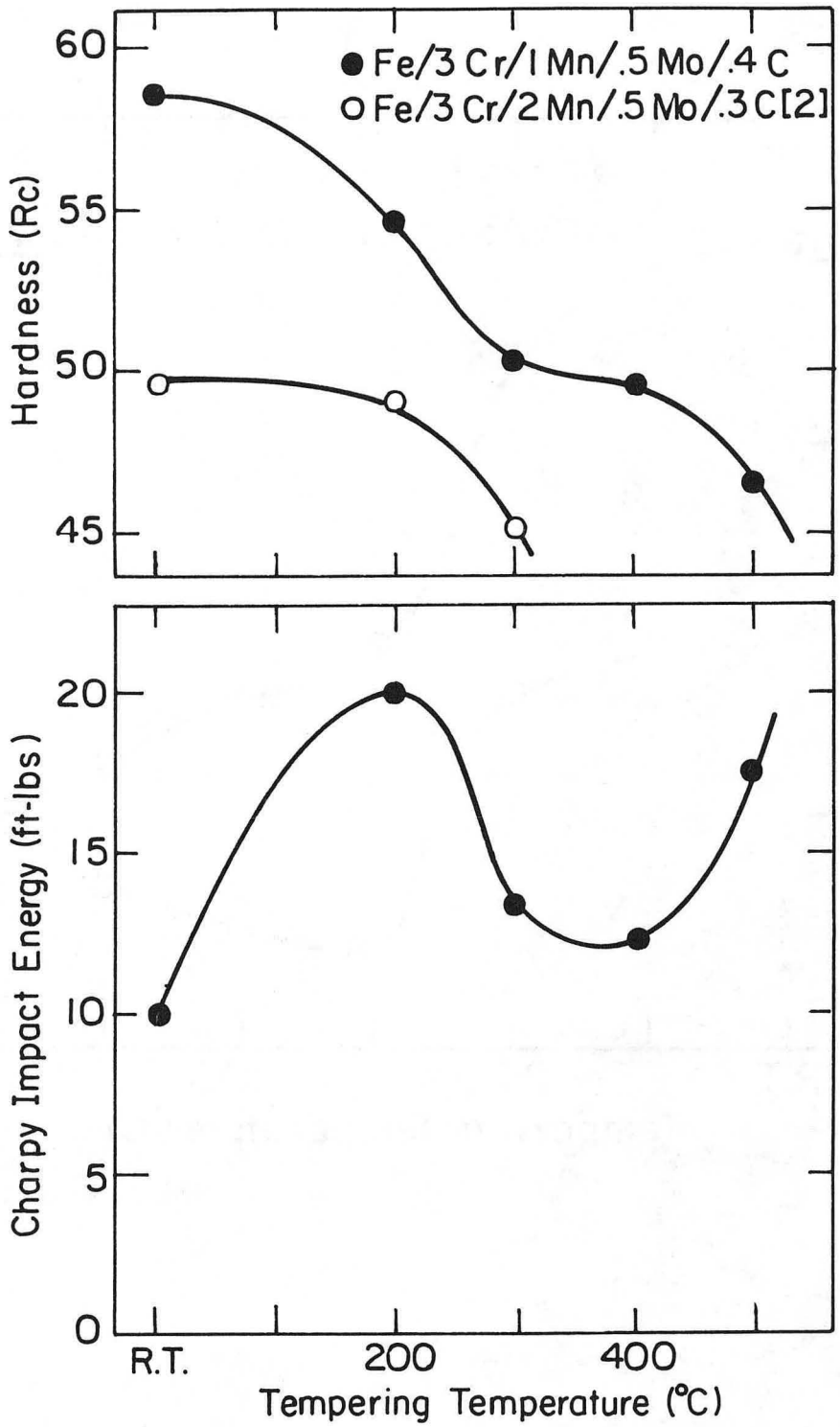
● Fe/3 Cr/1 Mn/.5 Mo/.4 C
○ Fe/3 Cr/2 Mn/.5 Mo/.3 C[2]
Hardness (Rc)
60
55
50
45
Charpy Impact Energy (ft-lbs)
20
15
10
5
0
R.T.
200
400
Tempering Temperature (°C)
XBL 837-6033

Fig. 12

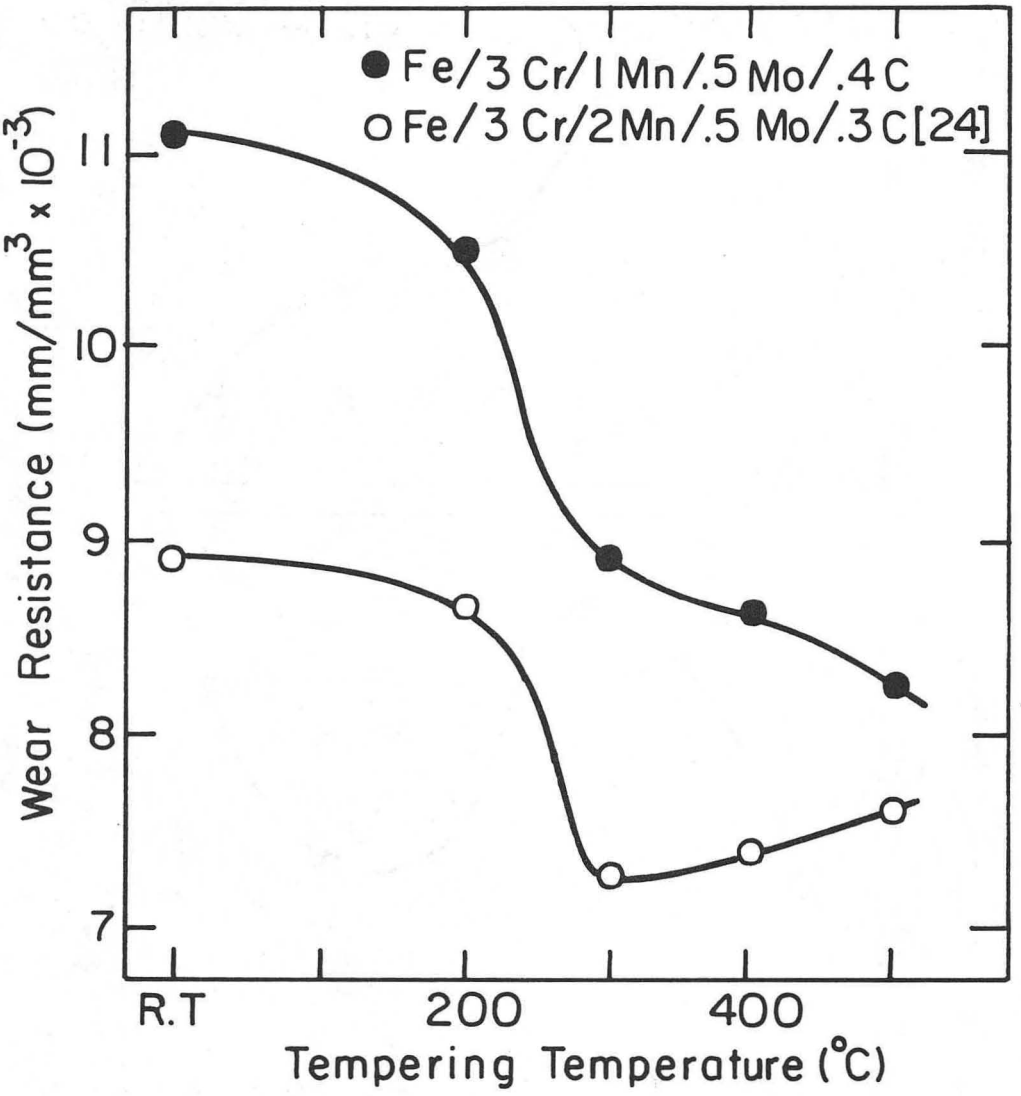
● Fe/3 Cr/1 Mn/.5 Mo/.4 C
○ Fe/3 Cr/2 Mn/.5 Mo/.3 C[24]
Wear Resistance (mm/mm³ x 10⁻³)
11
10
9
8
7
R.T
200
400
Tempering Temperature (°C)
XBL 837-6034

Fig. 13

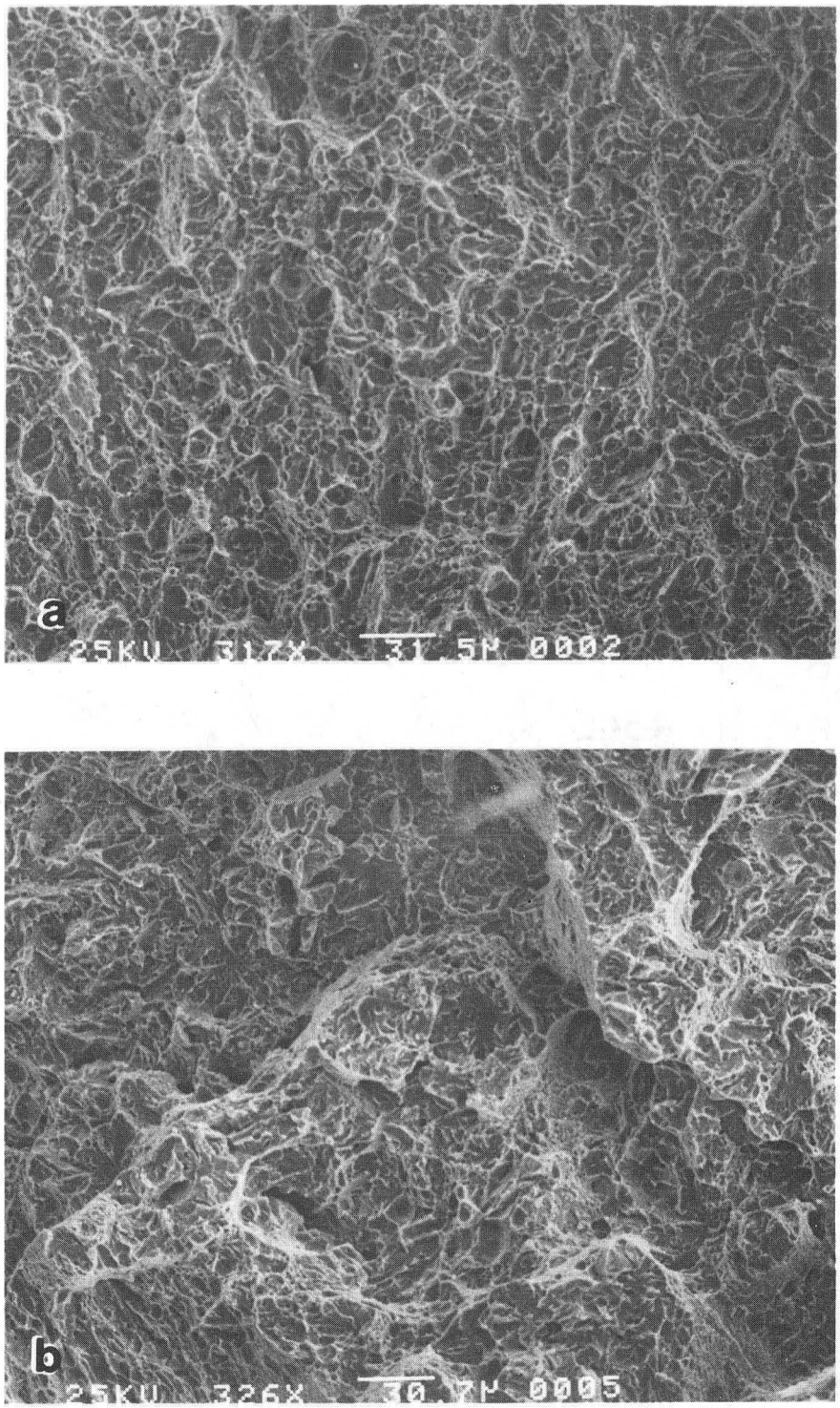

XBB 837-5996

Fig. 14

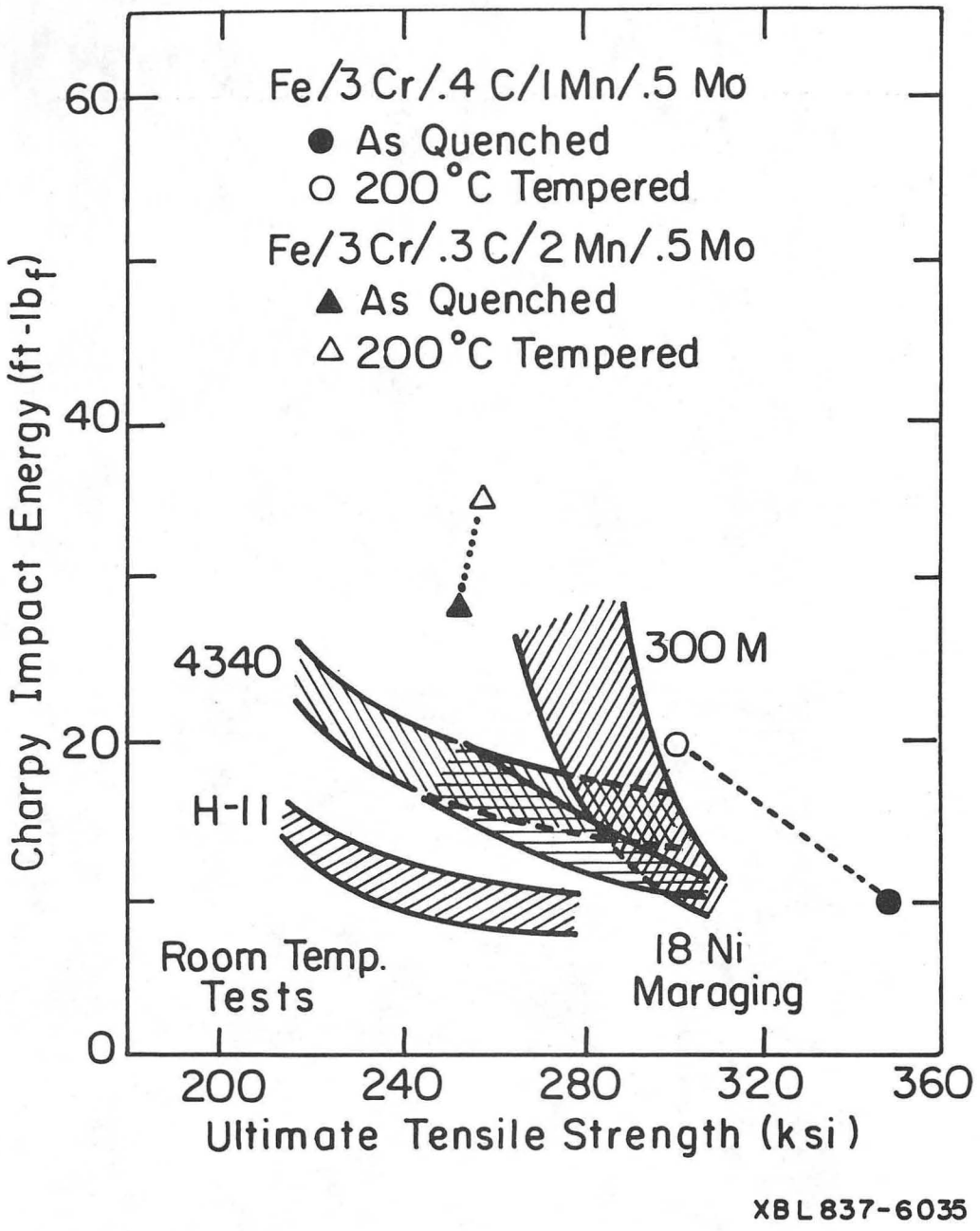
Fe/3 Cr/.4 C/1 Mn/.5 Mo
● As Quenched
○ 200°C Tempered
Fe/3 Cr/.3 C/2 Mn/.5 Mo
▲ As Quenched
△ 200°C Tempered
4340
300 M
H-11
18 Ni
Maraging
Room Temp.
Tests
Charpy Impact Energy (ft-lb$_f$)
Ultimate Tensile Strength (ksi)
0
20
40
60
200
240
280
320
360
XBL837-6035

Fig. 15(a)

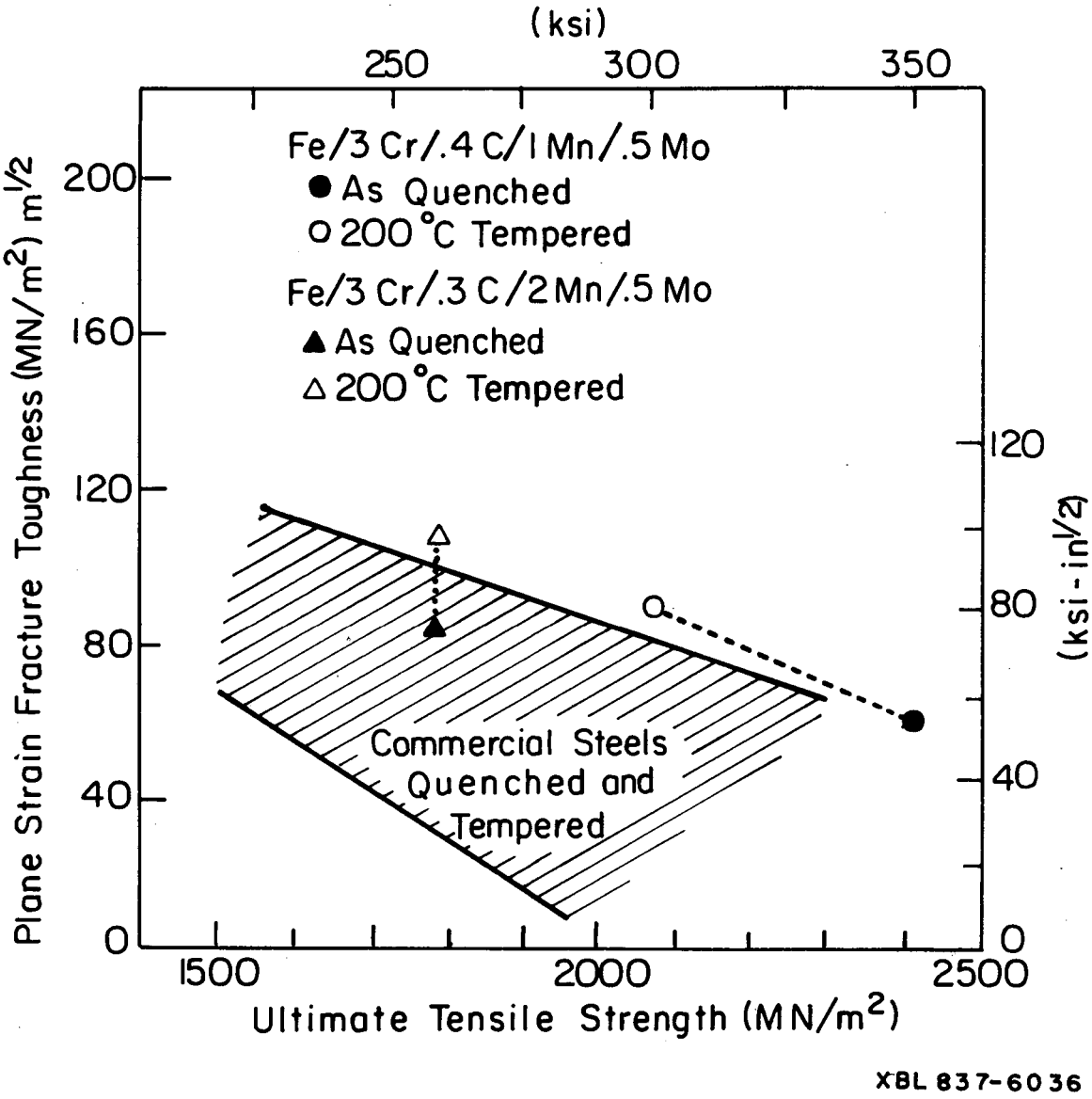
(ksi)
250
300
350
Fe/3 Cr/.4 C/1 Mn/.5 Mo
● As Quenched
○ 200 °C Tempered
Fe/3 Cr/.3 C/2 Mn/.5 Mo
▲ As Quenched
△ 200 °C Tempered
Commercial Steels
Quenched and
Tempered
Plane Strain Fracture Toughness (MN/m²) m^1/2
200
160
120
80
40
0
120
80
40
0
(ksi-in^1/2)
1500
2000
2500
Ultimate Tensile Strength (MN/m²)
XBL 837-6036

Fig. 15(b)

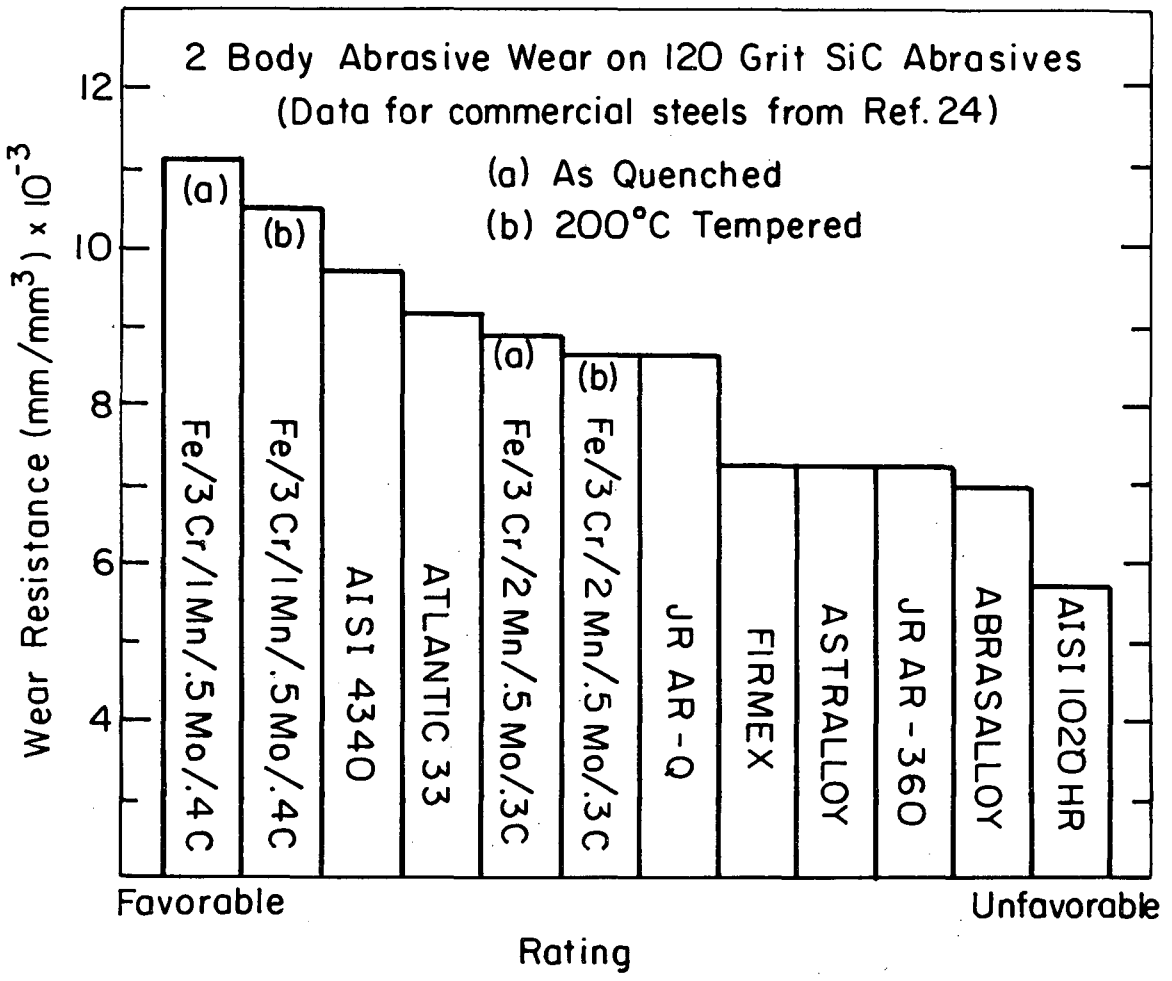
2 Body Abrasive Wear on 120 Grit SiC Abrasives
(Data for commercial steels from Ref. 24)
(a) As Quenched
(b) 200°C Tempered
Wear Resistance (mm/mm³) x 10⁻³
12
10
8
6
4
(a) Fe/3 Cr/1 Mn/.5 Mo/.4 C
(b) Fe/3 Cr/1 Mn/.5 Mo/.4 C
AISI 4340
ATLANTIC 33
(a) Fe/3 Cr/2 Mn/.5 Mo/.3 C
(b) Fe/3 Cr/2 Mn/.5 Mo/.3 C
JR AR-Q
FIRMEX
ASTRALLOY
JR AR-360
ABRASALLOY
AISI 1020 HR
Favorable
Unfavorable
Rating
XBL 837-6037

Fig. 16

TECHNICAL INFORMATION DEPARTMENT
LAWRENCE BERKELEY LABORATORY
UNIVERSITY OF CALIFORNIA
BERKELEY, CALIFORNIA 94720